INTERFACE

rsif.royalsocietypublishing.org

Research

**Cite this article:** Hong T, Fung ES, Zhang L, Huynh G, Monuki ES, Nie Q. 2015 Semi-adaptive response and noise attenuation in bone morphogenetic protein signalling. *J. R. Soc. Interface* **12**: 20150258. http://dx.doi.org/10.1098/rsif.2015.0258

Received: 23 March 2015
Accepted: 21 April 2015

**Subject Areas:**
systems biology, computational biology, biophysics

**Keywords:**
activation time, adaptive response, noise attenuation, response speed, negative feedback, SMAD phosphorylation

**Authors for correspondence:**
Edwin S. Monuki
e-mail: emonuki@uci.edu
Qing Nie
email: qnie@uci.edu

†These authors contributed equally to this work.

Electronic supplementary material is available at http://dx.doi.org/10.1098/rsif.2015.0258 or via http://rsif.royalsocietypublishing.org.

THE ROYAL SOCIETY PUBLISHING

# Semi-adaptive response and noise attenuation in bone morphogenetic protein signalling

Tian Hong[1,2,†], Ernest S. Fung[2,3,†], Lei Zhang[4], Grace Huynh[3], Edwin S. Monuki[2,3] and Qing Nie[1,2]

[1]Department of Mathematics, [2]Center for Complex Biological Systems, and [3]Department of Pathology and Laboratory Medicine, University of California, Irvine, CA, USA
[4]Beijing International Center for Mathematical Research, Peking University, Beijing, China

ESM, 0000-0001-5130-781X

Temporal dynamics of morphogen-driven signalling events are critical for proper embryonic development. During development, cells translate extracellular bone morphogenetic protein (BMP) gradients, often subject to noise, into graded intracellular tail-phosphorylated SMAD (TP-SMAD) levels. Using modelling and experimental approaches, we found that BMPs induce TP-SMAD responses in neural precursor cells in a concentration-dependent manner, which are semi-adaptive within a specific intermediate range of BMP concentration. These semi-adaptive TP-SMAD responses involve an intrinsically slow deactivation of BMP receptors, which attenuates noise by prolonging SMAD deactivation time after BMP withdrawal, but increases response time. Interestingly, negative feedback on BMP receptors is also required for semi-adaptation, which benefits both noise attenuation and response time, and therefore balances the trade-off seen with slow BMP receptor deactivation. These results highlight the rich dynamics of SMAD regulation in response to graded BMP concentration, and elucidate general design principles for balancing noise attenuation and activation speed in signalling systems.

## 1. Introduction

Bone morphogenetic proteins (BMPs) play critical roles in embryogenesis and tissue patterning [1–3]. As morphogens, BMPs regulate patterning by forming concentration gradients within developing tissues [4] and specify multiple cell fates in a concentration-dependent manner. Central to BMP-induced intracellular signalling is the activation of SMAD transcription factors [5–7]. BMPs activate SMADs 1, 5 and 8 by BMP receptor-mediated phosphorylation of C-terminal SMAD residues, thus forming tail-phosphorylated SMADs (TP-SMADs) that are imported into the nucleus to regulate transcription [6,8].

SMADs mediate a variety of BMP-induced cellular responses [9,10]. In neural precursor cells (NPCs) of the developing cerebral cortex, steady-state TP-SMAD levels form a dorsoventral gradient *in vivo* [11] and approximate extracellular BMP concentrations *in vitro* [12], suggesting that TP-SMAD is a direct and proportional readout of extracellular BMP concentration. (Although BMPs activate multiple SMADs, we focus here on SMAD1 for simplicity.) In addition to steady-state responses, pulse-like responses to morphogens can be critical for tissue development [13]. While BMPs can generate this type of response at the level of SMAD1 [10], the temporal dynamics of SMAD1 activation to graded BMP signals is poorly understood.

The processing of spatial information encoded by morphogens is subject to significant noise or fluctuations [14]. Mechanisms that attenuate BMP signalling noise are required for accurate interpretation [15,16]. The signalling cascade from BMP to TP-SMAD is controlled by a negative feedback loop, in which SMAD1 target genes neutralize BMPs or their interaction with BMP receptors [17–20]. While negative feedback can attenuate noise and maintain homeostasis [21,22], its roles in graded BMP signal responses are unclear.

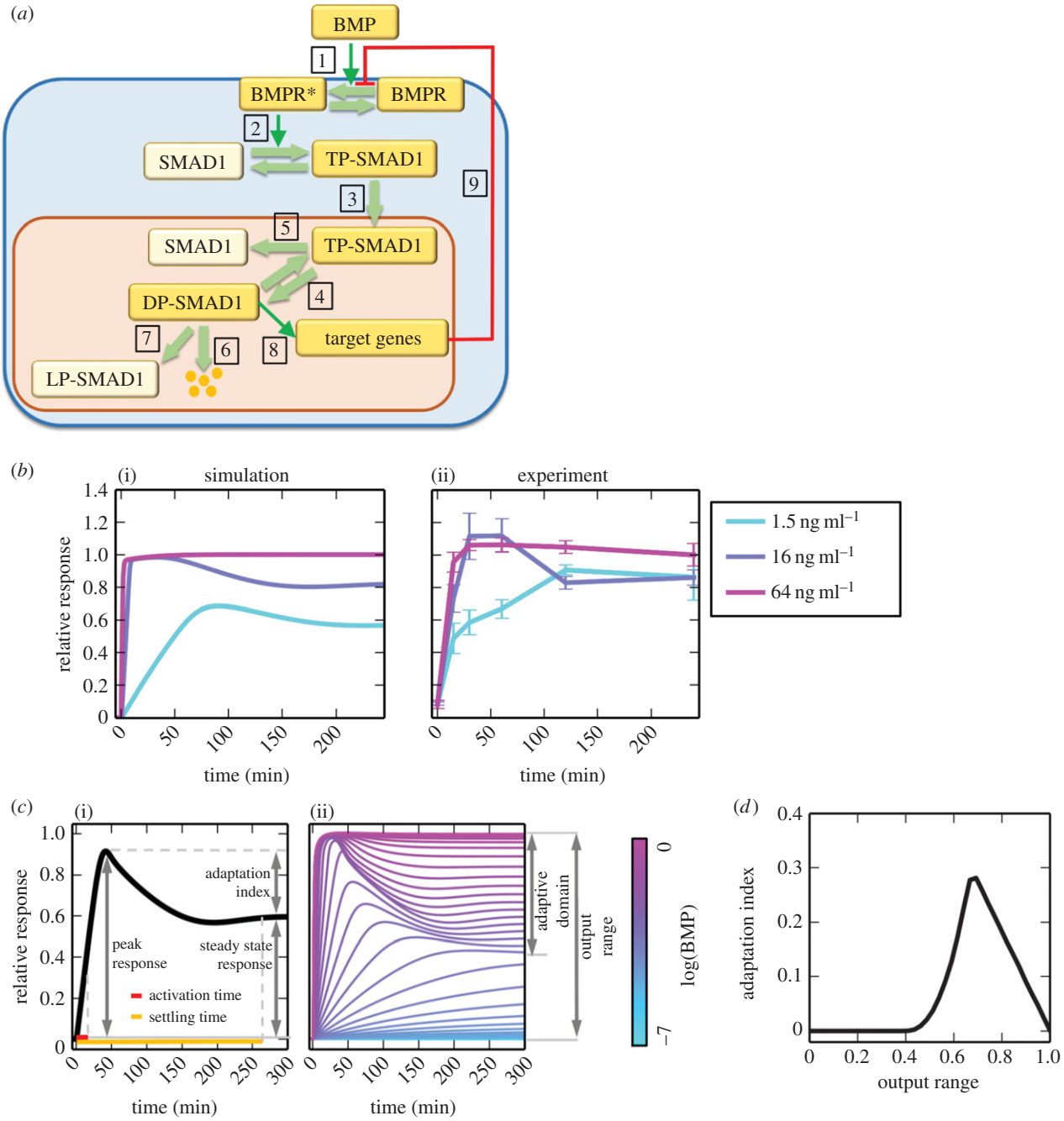


**Figure 1.** Dose-dependent dynamic responses to graded BMP signals. (*a*) Schematic of the BMP signalling pathway. Target gene-mediated negative feedback on BMP receptor activation is shown in red (edge no. 9). (*b*)(i) Simulations for low, intermediate and high doses of BMP. (ii) Western blot analysis on TP-SMAD1 during BMP4-induced activation. Cells were treated with indicated BMP4 concentrations at time zero, then lysed and analysed at indicated time points. We obtained 'relative response' by normalizing a group of trajectories to the maximum steady-state response in this group. (*c*)(i) Illustration of metrics used to describe responses. (ii) Simulations of TP-SMAD1 response for graded BMP signals (see colour code), starting with no BMP initially. (*d*) Adaptation index (AI, the difference between peak and steady-state response levels) with respect to the output range.

Here, we combine experimental and modelling approaches to investigate the dynamics of SMAD1 activation in NPCs responding to graded BMP signals. We show that an intermediate range of BMP concentration triggers semi-adaptive SMAD1 responses, which differ from the non-adaptive responses stimulated by higher or lower BMP levels and accelerate cell response. However, BMP receptor deactivation is slow, which benefits noise attenuation, but exhibits the trade-off of increasing response time. Interestingly, BMP receptor inhibition through negative feedback, which is required for the semi-adaptation, exhibits no such trade-off. Taken together, these findings define a cell-intrinsic control mechanism for creating fast adaptive responses with attenuated noise within a morphogen gradient.

## 2. Results

### 2.1. Dose-dependent dynamic responses to graded input BMP signals

To examine the dynamics of graded BMP signalling, we built a model based on current knowledge of the BMP signalling pathway (figure 1*a*; electronic supplementary material, table S1 and text). Simulations of the model showed two distinct types of responses. Low or high BMP concentrations induced a non-adaptive response (no significant decrease of response throughout the time frame; figure 1*b*(i)), whereas intermediate BMP concentrations gave rise to a semi-adaptive response in which TP-SMAD1 levels were significantly greater

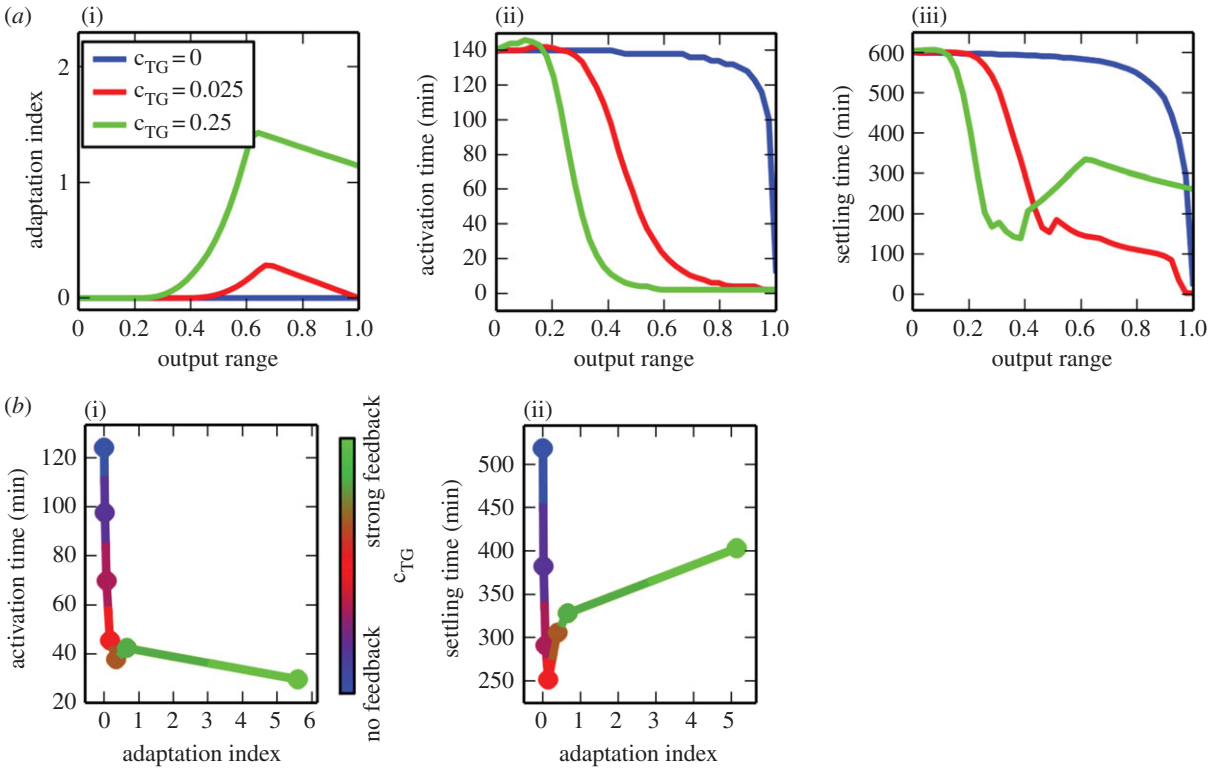


**Figure 2.** Characterization of semi-adaptive responses. (*a*) Comparison of open circuit/no negative feedback (blue), regular negative feedback (red) and strong negative feedback (light green) on adaptation index (AI) (i), activation time (ii) and settling time (iii) with respect to the output range. Rate of target genes production is varied to simulate different negative feedback strengths. (*b*) Relationships between mean AI and mean activation time (i) or mean settling time (ii) when strength of negative feedback is varied (see colour code). Each point represents a group of graded TP-SMAD1 responses to graded BMP signals. See electronic supplementary material, tables S2 for choices of parameters in the model.

earlier compared with later (i.e. an 'over-shooting' phenomenon; figure 1*b*(i)). In addition, the responses to intermediate and high BMP were generally rapid compared with those at low BMP concentration.

To investigate these dynamics experimentally, we treated E12.5 NPCs with low, intermediate and high BMP4 concentrations (1.5, 16 and 64 ng ml$^{-1}$) based on our previous studies [12,23] and measured TP-SMAD1 levels at various time points. Notably, we observed a semi-adaptive response at 16 ng ml$^{-1}$ BMP4, while non-adaptive responses were seen at 1.5 or 64 ng ml$^{-1}$. Moreover, activation at 1.5 ng ml$^{-1}$ BMP4 was slower than at the two higher concentrations (at 15 min, the mean responses were 0.45, 0.73 and 0.95 for BMP concentrations of 1.5, 16 and 64 ng ml$^{-1}$, respectively; figure 1*b*). These experimental results confirmed predictions made by the model regarding activation speed and semi-adaptive TP-SMAD1 responses as functions of BMP concentration.

We then defined new metrics to further analyse these responses (figure 1*c*). 'Adaptation index' (AI) represents the difference between peak and steady-state response levels (e.g. this index equals 0 for perfectly non-adaptive responses and greater than 0 for adaptive ones). 'Activation time' refers to the time needed to reach one-half of the steady-state response level. 'Settling time' is the time required to reach steady state, which is the state after which there is no more than 1% fluctuation in response levels. These metrics capture essential elements of the BMP-SMAD1 responses already described (figure 1*c*,*d*).

Using these metrics, we performed simulations with and without target gene-mediated negative feedback on the BMP receptor. We found that the decrease of TP-SMAD1 level is accompanied by an increase of the SMAD1 target gene products that are involved in the negative feedback (electronic supplementary material, figure S2*a*), and the presence and overall dynamics of the semi-adaptive response strongly depend on the negative feedback (electronic supplementary material, figure S2*b*; figure 2*a*(i)). In particular, the presence of negative feedback resulted in faster activation time (figure 2*a*(ii)), which was fastest in the adaptive domain (output range approx. 0.5–0.9; figure 1*c*(ii)). Settling times were also shorter in the adaptive region for intermediate-strength negative feedback (figure 2*a*(iii), red curve), but interestingly, settling time increased in the adaptive domain when negative feedback was strong (figure 2*a*(iii), green curve).

Overall, mean activation time was inversely dependent on mean AI (figure 2*b*(i)), whereas mean settling time had a biphasic relationship with mean AI—first decreasing, then increasing with higher negative feedback strength (figure 2*b*(ii)). Varying other parameters in the negative feedback loop, such as the strength of receptor inhibition, has similar effects (electronic supplementary material, figure S3). This suggests that negative feedback can be a key point of regulation for optimizing response speed.

## 2.2. Slow BMP receptor deactivation attenuates noise by slowing SMAD1 deactivation, but increases response time

We next studied how temporal fluctuations (noise) in BMP affect the semi-adaptive responses. Previous studies have shown that noise attenuation is associated with signed activation time (SAT) [24], defined as the difference between deactivation time (deactivation time is defined as the time

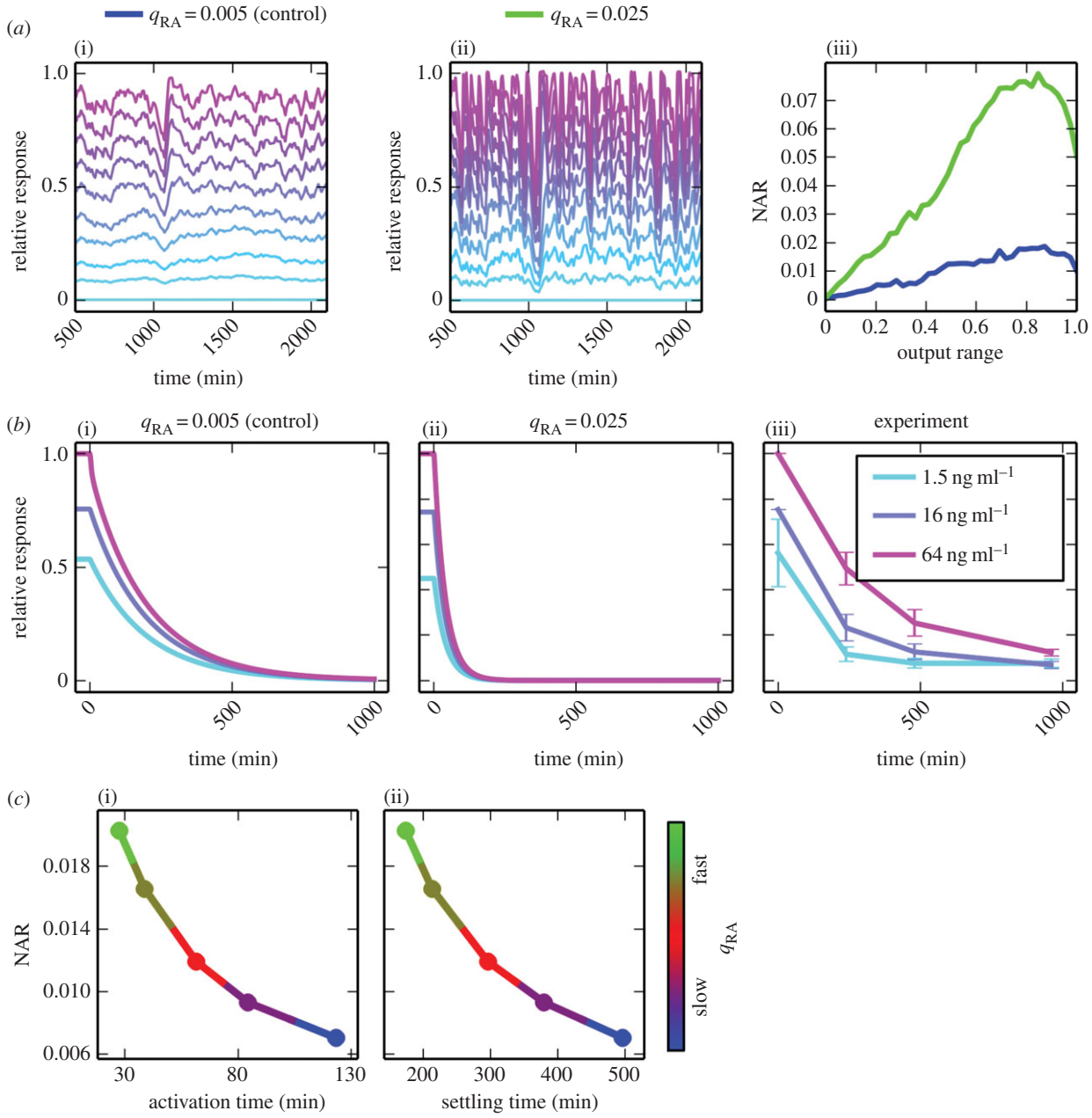


**Figure 3.** Slow deactivation of BMP receptor attenuates noise, but increases response time. (*a*) Sample trajectories of steady-state TP-SMAD1 from each domain of responses for slow (i) and fast (ii) receptor deactivation. (iii) Noise amplification rate (NAR) of each domain of responses for the two scenarios. (*b*)(i) and (ii) Sample simulation trajectories of TP-SMAD1 upon withdrawal of BMP. Simulations began at TP-SMAD1 steady states induced by three different BMP doses before dropping BMP levels to zero at time zero. (iii) Western blot analysis on TP-SMAD1 after BMP washout. Cells were treated with three different BMP4 doses for 2 h, triple washed, then BMP-free medium was replaced at time zero. Cells were lysed and analysed at indicated time points. (*c*) Relationships between mean NAR and mean activation time (i) or mean settling time (ii) when receptor deactivation rate is varied (see colour code). Each data point represents a group of graded TP-SMAD1 responses to graded BMP signals. See tables S2 for choices of parameters in the model.

needed to reach one-half of the steady-state response level) upon signal withdrawal and activation time upon signal engagement (see Material and methods for details on computing SAT), with larger SAT values leading to smaller values of 'noise amplification rate' (NAR, see Material and methods) [24,25]. To study SAT–NAR relationships, we perturbed each parameter in the BMP model and examined the effects on SAT and NAR. We observed an inverse SAT–NAR relationship for TP-SMAD1 (electronic supplementary material, figure S4)—i.e. smaller SAT values led to larger NAR values. Interestingly, perturbation of BMP receptor deactivation rate ($q_{RA}$) had the most prominent effect on SAT and NAR values (electronic supplementary material, figure S4), suggesting a critical role for receptor deactivation in noise attenuation. A high BMP receptor deactivation rate (large $q_{RA}$ value) yielded small SAT values and high NARs, i.e. large response fluctuations (electronic supplementary material, figure S4; figure 3*a*(ii and iii)).

To experimentally investigate TP-SMAD1 deactivation kinetics, we treated E12.5 NPCs with BMP4 for 2 h, then removed BMP4 and measured TP-SMAD1 levels over time. Consistent with the modelling results (figures 3*b*(i) and 1*b*(i)), the abundance of TP-SMAD1 decreased with a much slower rate upon BMP withdrawal than the activation rate upon BMP treatment (figures 3*b*(iii) and 1*b*(ii)), suggesting that the system is using slow receptor deactivation as a strategy to attenuate external BMP fluctuations.

While slow receptor deactivation can increase SAT and decrease NAR, it can also slow down response time for the semi-adaptation, as the mean NAR is inversely related to

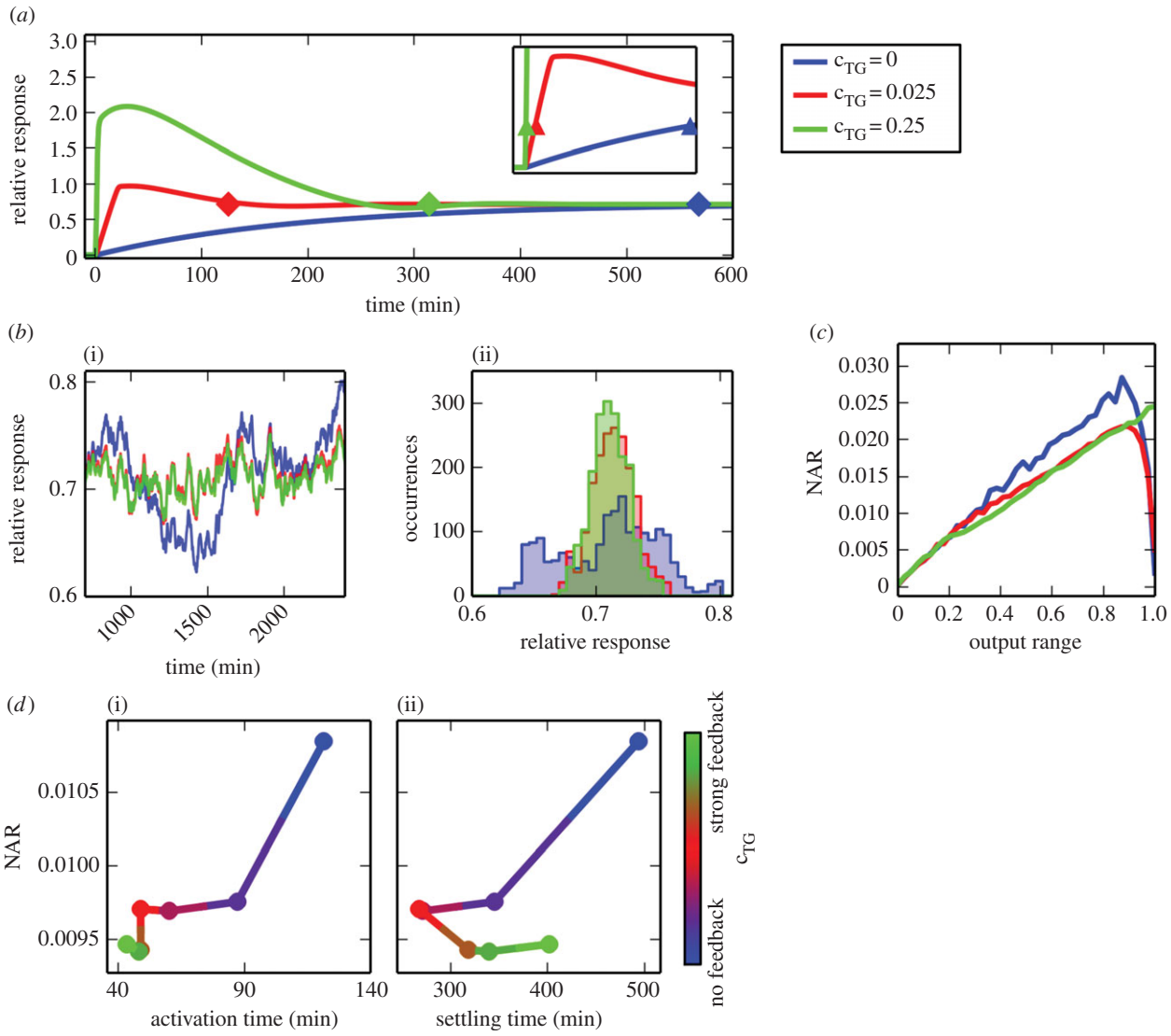


**Figure 4.** Negative feedback attenuates noise and decreases response time. (*a*) Three trajectories that give similar steady-state responses. Blue: open circuit/no negative feedback, no adaptation; red: regular negative feedback, moderate adaptation; light green: strong negative feedback, strong adaptation. Diamond marker: settling time point. Inset: three responses with distinct activation times labelled as triangles. (*b*)(i) Trajectories of TP-SMAD1 subject to fluctuating BMP signals under the same conditions in (*a*). (ii) Histogram of the three trajectories showing the distributions of the response levels in a 1000 min window. (*c*) Comparison of the three circuits on noise amplification rate (NAR) with respect to the output range. (*d*) Relationships between mean NAR and mean activation time (i) or mean settling time (ii) when strength of negative feedback is varied. Each data point represents a group of graded TP-SMAD1 responses to graded BMP signals. See tables S2 for choices of parameters in the model.

activation time as well as settling time (figure 3*c*). This indicates a trade-off between fast activation and noise attenuation in the presence of slow BMP receptor deactivation.

## 2.3. Negative feedback can increase activation speed and attenuates noise

To investigate the role of negative feedback in noise attenuation, we selected three typical responses with similar steady states, but distinct adaptation indices due to different negative feedback strengths (figure 4*a*). With fluctuating BMP inputs, we observed the non-adaptive response had greater fluctuations at its steady states than the two adaptive responses (figure 4*a*,*b*, compare blue lines to others), and the two adaptive responses had similar fluctuations (figure 4*a*,*b*, red and light green).

We found that negative feedback mainly decreased NAR in the intermediate output range (figure 4*c*, red and light green curves compared to blue curve), and negative feedback strength had a positive relationship with mean activation time and a biphasic relationship with mean settling time (figure 4*d*; electronic supplementary material, figure S6), suggesting that negative feedback can shorten the activation time significantly and attenuate noise moderately. To compare negative feedback with the slow receptor deactivation in terms of how they attenuated noise, we selected a case in which two parameter sets (figure 5*a*, blue and green curves; compare them with red curve as a control), representing negative feedback and slow receptor deactivation, respectively, produced similar levels of mean response and output noise (figure 5*b*). Negative feedback sped up SMAD1 activation significantly (figure 5*a*, upright triangles). By contrast, slow receptor deactivation slowed down SMAD1 deactivation significantly (figure 5*a* inverted triangles). This suggests that the two strategies (negative feedback and slow receptor deactivation) increased SAT and attenuated noise with distinct mechanisms. Since slow receptor deactivation slowed activation time, to balance speed and noise attenuation, it must be combined with other strategies, such as negative feedback, to ensure fast activation speed. As expected, combining the

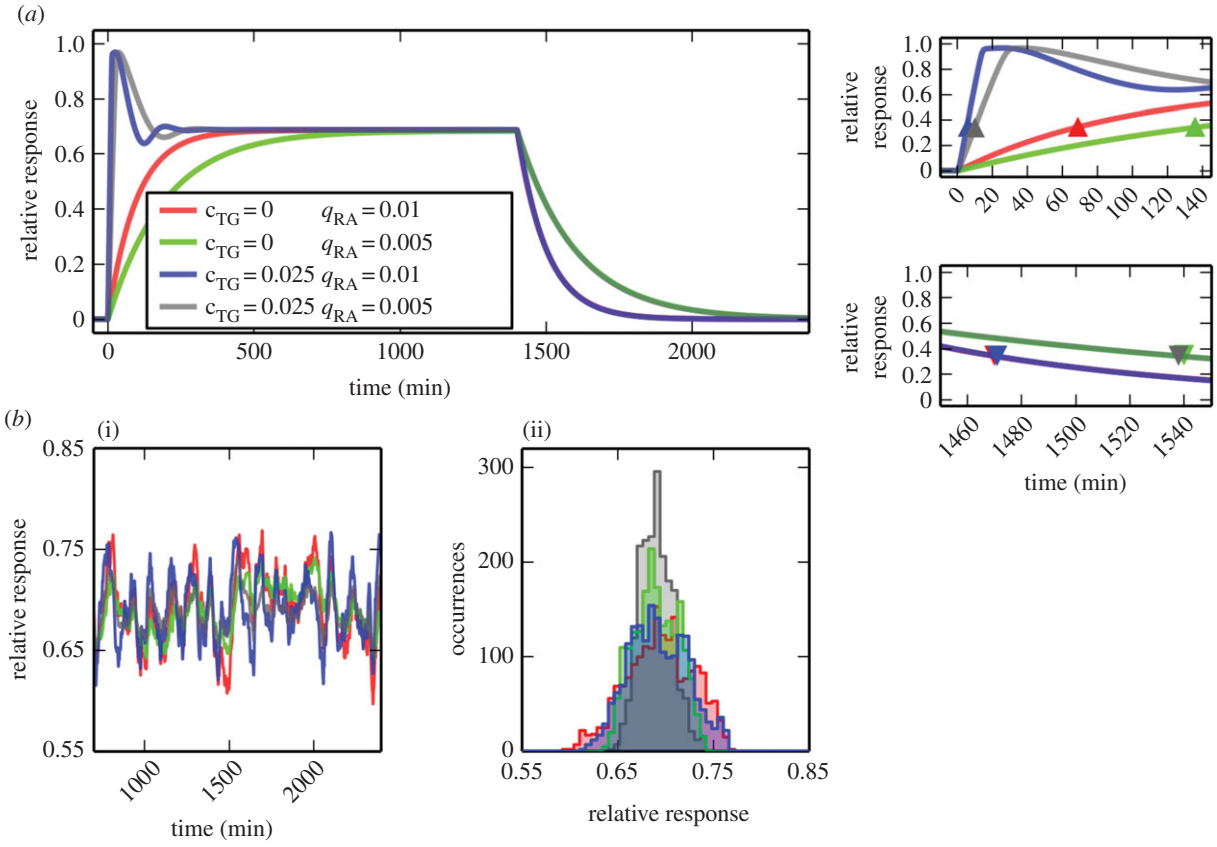


**Figure 5.** Comparison of negative feedback and slow deactivation of BMP receptor on response speed and noise attenuation. (*a*) Four trajectories that give similar steady-state responses. Blue: negative feedback with fast receptor deactivation; red: open circuit with fast receptor deactivation; light green: open circuit with slow receptor deactivation; grey: negative feedback with slow receptor deactivation. Upper right: activation time (triangles). Lower right: deactivation time (triangles). (*b*)(i) Trajectories subject to fluctuating BMP signals under the same conditions in (*b*). (ii) Histogram of the three trajectories showing the distributions of the response levels in a 1000 min window.

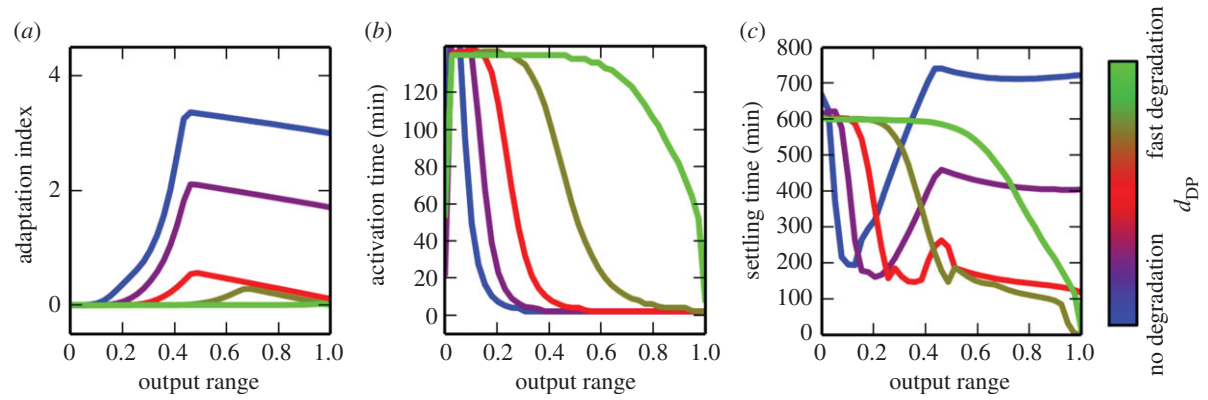


**Figure 6.** Effect of nuclear DP-SMAD1 degradation on semi-adaptive response. Comparison of five values of nuclear DP-SMAD1 degradation rates ($d_{DP}$) on adaptation index of TP-SMAD1 (*a*), activation time (*b*) and settling time (*c*) with respect to the output range.

two strategies produced a fast response with good noise attenuation properties (figure 5, grey curves).

## 2.4. Nuclear SMAD degradation controls the domain of semi-adaptive responses

It has been observed that nuclear linker-phosphorylation of SMAD1 triggers its proteasome-mediated degradation [26]. To understand the role of this regulation, we examined the effect of nuclear DP-SMAD1 degradation on response dynamics (edge 6 in figure 1*a*). As seen in the previous sections, strong negative feedback can increase the AI, but this effect is restricted to a specific range of output, and the adaptive domain did not change significantly with the feedback strength (figure 2*a*). Interestingly, varying the rate of nuclear DP-SMAD1 degradation altered the adaptive domain over the entire output range (figure 6; electronic supplementary material, figure S7). When degradation rate was low, almost the entire output range was adaptive (figure 6*a*, blue curve). Increasing the degradation rate restricted the adaptive domain to higher output ranges (figure 6*a*, purple, red and olive curves), and with very high degradation rates, adaptive behaviour was compromised and responses generally became non-adaptive (figure 6*a*, light green curves); this was due to the loss of negative feedback (not shown).

Similar to its effect on the adaptive domain, DP-SMAD1 degradation rate regulated response speeds: changing degradation rate resulted in the change of response domains in which fast response is achieved (figure 6*b*). In general, rapid DP-SMAD1 degradation slowed down the responses (figure 6*b*, green curve), and slower degradation rate expanded the fast-response domain towards the lower output range (figure 6*b*, olive, red, purple and blue curves). These results suggest that the DP-SMAD1 degradation must be controlled in order to produce adaptive dynamics and fast response in a defined range of the output. Moreover, intermediate degradation rate decreased the settling time, which is generally shorter than those obtained with fast or slow degradation rates (figure 6*c*, cf. red curve with others). This implies that the degradation rate might be optimized to shorten the time that the system takes to reach steady state. Varying DP-SMAD1 degradation rate did not have a pronounced effect on the noise attenuation (electronic supplementary material, figure S8). Overall, we suggest that the observed DP-SMAD1 degradation mediated by proteasome could be a strategy to control the dynamics of graded responses to graded signals.

## 3. Discussion

Previous theoretical studies have revealed interesting dynamic behaviours of TGF-β signalling networks [19,27–29], including adaptive responses. Mathematical models concerning BMP signalling mainly focused on receptor dynamics [30] or steady-state behaviour of mutual-inhibition loops [23]. However, temporal dynamics of the BMP signalling network including intracellular molecules and its role in noise attenuation have not been studied. With a new mathematical model for the BMP signalling network and experimental findings, we showed that the regulatory system for processing graded BMP signals has unique dynamic behaviours and noise attenuation strategies that have not been examined previously.

Our study revealed a variety of temporal dynamics, including the semi-adaptive responses produced through a negative feedback through TP-SMAD1, in BMP signalling. Other mechanisms such as regulated receptor trafficking in TGF-β pathway [31] or three-state regulation on signalling molecule IKK in NFκB signalling [32,33] may also lead to adaptive responses. Negative feedback is known for its role in reducing fluctuations [22] and speeding up cellular responses [34]. Our work demonstrates that the two roles of negative feedback can be connected in a single framework. In addition, negative feedback can produce oscillatory behaviours [35]. Although we did not observe any sustained oscillation in our simulations, we can reconcile the temporal variation arising from oscillation and the seemingly contradictory effect on the noise attenuation by the observation that strong negative feedback prolonged the settling time, i.e. the effect of noise attenuation at steady state can be masked by the increased time to reach the steady state (note that the settling time for sustained oscillation is infinite).

It has been suggested that negative feedback loop and enhanced degradation rate are two strategies for accelerating the response to external signals [34,36,37], partially responsible for the observed fast activation by BMP—an important feature for timely tissue development. Interestingly, our simulations suggest that high degradation rate sometimes reduces the effect of negative feedback, slowing down the response. This implies that a crosstalk and synergy of the two regulatory components are needed to control the speed of response.

Our result that slow deactivation rate of the receptor kinase is important for reducing fluctuations of the responses suggests that morphogens need long durations of occupancy when binding to their receptors. This is consistent with the previous studies showing that the slow deactivation in morphogen–receptor interaction allows the cells more sensitive to increase of morphogens than decrease of morphogens [38–40], highlighting the importance of slow deactivation in coupling with fast activation as an effective strategy in noise attenuation.

Signalling events in individual cells are influenced by noise in myriad ways: their external environments may fluctuate in space and time, their internal properties (e.g. levels of gene expression) may differ from cell to cell (i.e. variability) even in a monoclonal population, and molecular fluctuations exist in single cells owing to small numbers of regulatory genes, mRNAs and proteins. In this study, we focused on the attenuation strategy for fluctuations of a morphogen (BMP) that plays an important role in specifying spatial information and acting as a stimulus for downstream responses in a cell. Noise in morphogen systems might be a major source for the roughness of boundaries in early stages of patterning by morphogen gradients [16], and the noisy spatial distribution of the morphogen has been observed in experiments at various stages of development [14]. Nonetheless, cells are inevitably interfered by other sources of noise at various levels in addition to noise in morphogens, and different noise attenuation strategies are then needed to reduce the overall stochastic effect during cell signalling.

Overall, our findings on cell-intrinsic dynamics during telencephalon development suggest a mechanism that can balance response speed and noise attenuation when multiple performance objectives are taken into consideration. It requires further study to integrate such mechanism centred at SMAD into BMP signalling pathways to explore its role in the cascades of signal transduction stimulated by BMP signals that contain spatial information and noise.

## 4. Material and methods

### 4.1. Mice

Noon of the vaginal plug date was designated as day 0.5 for timed pregnancies. Crown–rump length was measured to verify embryonic ages.

### 4.2. E12.5 dissociated neuronal precursor cell cultures

The cultures were performed as previously described [12,23]. Briefly, E12.5 embryos were dissected, then skin and mesenchymal layers were removed from the head to expose the developing telencephalon. Dorsal portions of the telencephalic vesicles were harvested and incubated in 0.05% trypsin with 0.02% EDTA and 0.2% BSA in HBSS for 20 min at 37°C for dissociation; 1 mg $ml^{-1}$ soy bean trypsin inhibitor (Sigma) in HBSS was used to inhibit trypsin after dissociation. Tissues were pipetted up and down to dissociate cells using P200 pipette. Cells were then washed once with 0.2% BSA in HBSS and plated at 500 000 cells per well on laminin-coated plates.

### 4.3. BMP activation and deactivation experiments

Twenty-four hours after plating, varying amounts of BMP4 (R&D Systems) were added to the cultures. For the activation

experiments, the time of BMP4 addition represented time zero. For the deactivation experiments, varying amounts of BMP4 were added to the cultures after the initial 24 h plating period. Two hours after BMP4 treatment (which ensured attainment of TP-SMAD1 steady state; see figure 1*b*(ii)), triple washout with BMP-free media was performed, then BMP4-free media was applied at time zero. Protein was extracted at specified time points after BMP4 addition (activation, figure 1*b*) or after BMP4 washout (deactivation, figure 2*b*).

## 4.4. Protein extraction and LI-COR/Odyssey Western blot

Protein extraction was performed using RIPA lysis buffer supplemented with protease inhibitor cocktail (Roche) and phosphatase inhibitor cocktail (Roche). Lysis buffer was applied to cells; cell lysate was collected and incubated on ice for 10 min. Lysate was centrifuged at 10 000 g for 15 min and supernatant was transferred and stored at −80°C for further analysis. Laemmli sample buffer (BioRad) was added to protein sample and run on 7.5% Mini-Protean TGX gel (BioRad) in Tris Glycine SDS buffer (BioRad). Sample was transferred onto 0.45 um nitrocellulose membrane (BioRad) in Tris Glycine transfer buffer overnight. Primary antibodies used: β-actin (Cell Signalling; 8H10D10) and pSmad 1,5,8 (Chemicon; AB3848). Secondary antibodies used: IR Dye 680LT anti-rabbit IgG and IR Dye 800 CW anti-mouse IgG (LI-COR). Membranes were scanned and quantified using Odyssey IR scanner (LI-COR). Results were normalized to β-actin and plotted as a fraction of maximal TP-SMAD1 levels.

## 4.5. Mathematical model and simulations

We used ordinary differential equations to describe the interactions of the molecules involved in BMP signalling pathways (electronic supplementary material, figure S1). Based on a few assumptions, we simplified the known interactions into a core regulatory network (electronic supplementary material, text). The influence diagram of the network is shown in figure 1*a*. Equations, parameter values used for simulations and detailed descriptions of quantities and model assumptions can be found in the electronic supplementary material.

To ensure relevance to the BMP concentrations used and the TP-SMAD1 responses observed, we ran many simulations with varying BMP intensities and made sure that (i) maximum steady-state TP-SMAD1 response was significantly different from background, (ii) sufficient number of BMP intensities were used, such that at least one response could be put in a bin spanning one-tenth of the space between the minimum and maximum response, thus allowing for the analysis of 10 bins with varying intensities (we refer to these bins as 'response domains'), and (iii) sufficient maximum doses of BMP were used so that any distinct high BMP responses were not missed. After a group of graded responses were obtained, we normalized the trajectories with the maximum steady-state response in the group (i.e. relative responses).

## 4.6. Adaptation index

The AI is defined as the following:

$$\mathrm{AI} = \frac{c_\mathrm{p} - c_\mathrm{s}}{c_1 - c_0}, \tag{4.1}$$

where $c_\mathrm{p}$ is the maximum response (peak) and $c_\mathrm{s}$ is the steady-state response. $c_0$ and $c_1$ are the minimum and maximum steady-state responses to the graded signal, respectively (see below).

## 4.7. Signed activation time

We defined SAT as the following:

$$\mathrm{SAT} = t_\mathrm{off} - t_\mathrm{on},$$

where $t_\mathrm{off}$ is the deactivation time, i.e. the time needed for the response to reach one-half of the steady-state response level from its maximum steady-state level upon signal withdrawal, and $t_\mathrm{on}$ is the activation time, i.e. the time needed for the response to reach one-half of the steady-state response level from its maximum steady-state level upon signal engagement. In our original definition of SAT, SAT is normalized by the inverse of the frequency in the signal [24]. Since the noise frequency is a constant ($1\ \mathrm{h}^{-1}$) in all of our simulations, we did not consider this normalization in this study.

To obtain $t_\mathrm{on}$ and $t_\mathrm{off}$, we first defined the following time points at which the value of BMP signal was changed during a simulation:

$t_0$: time point at the beginning of the simulation (BMP signal is off);
$t_1$: time point at which BMP signal is turned on;
$t_2$: time point at which BMP signal is turned off.

We performed simulations without BMP signal so that the system was first stabilized at its 'off' steady state (from $t_0$ to $t_1$). Next, we changed BMP signal to a positive value at $t_1$ and continued the simulations so that the system was stabilized at its 'on' steady state (from $t_1$ to $t_2$). From the simulation trajectories obtained here, we estimated $t_\mathrm{on}$. We next changed BMP signal to zero again at $t_2$ and continued the simulations so that the system reached its 'off' state again. We estimated $t_\mathrm{off}$ based on the trajectories after $t_2$. We chose $t_1 = 100$ min, $t_2 = 1400$ min for this model to ensure that the steady states were reached.

## 4.8. Noise amplification rate

The temporal fluctuations and NAR are based on the previous studies [24,25]. In particular, we define

$$\mathrm{NAR} = \frac{\mathrm{std}(c)/(c_1 - c_0)}{\mathrm{std}(u)/\langle u \rangle}, \tag{4.2}$$

where $c$ is the level of response (TP-SMAD1) to a particular signal input $u$ at steady state in a time period of 1000 min. $c_0$ and $c_1$ are the minimum and maximum steady-state responses to the graded signal, respectively. std(·) denotes the standard deviation, and $\langle \cdot \rangle$ denotes the mean. The coefficient of variance of the input signal is identical for all signal levels that we used. The mean NAR is defined as the mean of the NARs of the 10 representative responses from 10 graded response domains.

## 4.9. Sensitivity analysis

To screen for the parameters that have the most influence on NAR, activation time and deactivation time, we perturbed each parameter and checked the resulting change in these quantities. In each perturbation, we first increased a parameter by fivefold and ran a set of simulations with graded BMP signals, and then reduced the parameter by fivefold and ran another set of simulations. Subsequently, we computed the differences of the three quantities between the two sets of simulations for each one of the ten response domains. A positive change upon perturbation means the quantity increases with increasing a particular parameter value.

Ethics statement. Breeding colonies were established under IACUC breeding guidelines.

Acknowledgements. The authors thank the three anonymous reviewers for their insightful and constructive comments, which helped us to improve the manuscript.

Funding statement. This study was partially supported by NIH grants P50GM76516 (Q.N. and E.M.), R01GM107264 (Q.N.), R01DE023050 (Q.N.), R01NS064587 (E.M.), and NSF grant DMS1161621 (Q.N.).

Authors' contributions. T.H. performed the modelling work; E.F. and G.H. performed the experimental work; L.Z. contributed reagents; T.H., Q.N., E.F. and E.M. designed the study and wrote the paper.

Conflict of interests. The authors declare that they have no conflict of interest.

# References


1. Hogan BL. 1996 Bone morphogenetic proteins: multifunctional regulators of vertebrate development. *Genes Dev.* **10**, 1580–1594. (doi:10.1101/gad.10.13.1580)
2. Mehler MF, Mabie PC, Zhang D, Kessler JA. 1997 Bone morphogenetic proteins in the nervous system. *Trends Neurosci.* **20**, 309–317. (doi:10.1016/S0166-2236(96)01046-6)
3. Schier AF, Talbot WS. 2005 Molecular genetics of axis formation in zebrafish. *Annu. Rev. Genet.* **39**, 561–613. (doi:10.1146/annurev.genet.37.110801.143752)
4. Ferguson EL, Anderson KV. 1992 Decapentaplegic acts as a morphogen to organize dorsal-ventral pattern in the Drosophila embryo. *Cell* **71**, 451–461. (doi:10.1016/0092-8674(92)90514-D)
5. Shi Y, Massague J. 2003 Mechanisms of TGF-β signaling from cell membrane to the nucleus. *Cell* **113**, 685–700. (doi:10.1016/S0092-8674(03)00432-X)
6. Massague J, Seoane J, Wotton D. 2005 Smad transcription factors. *Genes Dev.* **19**, 2783–2810. (doi:10.1101/gad.1350705)
7. Xu L. 2006 Regulation of Smad activities. *Biochim. Biophys. Acta* **1759**, 503–513. (doi:10.1016/j.bbaexp.2006.11.001)
8. Feng X-H, Derynck R. 2005 Specificity and versatility in TGF-β signaling through Smads. *Annu. Rev. Cell Dev. Biol.* **21**, 659–693. (doi:10.1146/annurev.cellbio.21.022404.142018)
9. Sapkota G, Alarcon C, Spagnoli FM, Brivanlou AH, Massague J. 2007 Balancing BMP signaling through integrated inputs into the Smad1 linker. *Mol. Cell* **25**, 441–454. (doi:10.1016/j.molcel.2007.01.006)
10. Knockaert M, Sapkota G, Alarcon C, Massague J, Brivanlou AH. 2006 Unique players in the BMP pathway: small C-terminal domain phosphatases dephosphorylate Smad1 to attenuate BMP signaling. *Proc. Natl Acad. Sci. USA* **103**, 11 940–11 945. (doi:10.1073/pnas.0605133103)
11. Cheng X, Hsu C-M, Currle DS, Hu JS, Barkovich AJ, Monuki ES. 2006 Central roles of the roof plate in telencephalic development and holoprosencephaly. *J. Neurosci.* **26**, 7640–7649. (doi:10.1523/JNEUROSCI.0714-06.2006)
12. Hu JS, Doan LT, Currle DS, Paff M, Rheem JY, Schreyer R, Robert B, Monuki ES. 2008 Border formation in a Bmp gradient reduced to single dissociated cells. *Proc. Natl Acad. Sci. USA* **105**, 3398–3403. (doi:10.1073/pnas.0709100105)
13. Balaskas N, Ribeiro A, Panovska J, Dessaud E, Sasai N, Page KM, Briscoe J, Ribes V. 2012 Gene regulatory logic for reading the Sonic Hedgehog signaling gradient in the vertebrate neural tube. *Cell* **148**, 273–284. (doi:10.1016/j.cell.2011.10.047)
14. Shimozono S, Iimura T, Kitaguchi T, Higashijima S-I, Miyawaki A. 2013 Visualization of an endogenous retinoic acid gradient across embryonic development. *Nature* **496**, 363–366. (doi:10.1038/nature12037)
15. Schilling TF, Nie Q, Lander AD. 2012 Dynamics and precision in retinoic acid morphogen gradients. *Curr. Opin. Genet. Dev.* **22**, 562–569. (doi:10.1016/j.gde.2012.11.012.Dynamics)
16. Zhang L, Radtke K, Zheng L, Cai AQ, Schilling TF, Nie Q. 2012 Noise drives sharpening of gene expression boundaries in the zebrafish hindbrain. *Mol. Syst. Biol.* **8**, 613. (doi:10.1038/msb.2012.45)
17. Onichtchouk D, Chen YG, Dosch R, Gawantka V, Delius H, Massagué J, Niehrs C. 1999 Silencing of TGF-β signalling by the pseudoreceptor BAMBI. *Nature* **401**, 480–485. (doi:10.1038/46794)
18. Massague J, Chen YG. 2000 Controlling TGF-β signaling. *Genes Dev.* **14**, 627–644. (doi:10.1101/gad.14.6.627)
19. Nicklas D, Saiz L. 2013 Characterization of negative feedback network motifs in the TGF-β signaling pathway. *PLoS ONE* **8**, e83531. (doi:10.1371/journal.pone.0083531)
20. Sun Q, Mao S, Li H, Zen K, Zhang C-Y, Li L. 2013 Role of miR-17 family in the negative feedback loop of bone morphogenetic protein signaling in neuron. *PLoS ONE* **8**, e83067. (doi:10.1371/journal.pone.0083067)
21. Thomas R, Thieffry D, Kaufman M. 1995 Dynamical behaviour of biological regulatory networks—I. Biological role of feedback loops and practical use of the concept of the loop-characteristic state. *Bull. Math. Biol.* **57**, 247–276. (doi:10.1007/BF02460618)
22. Dublanche Y, Michalodimitrakis K, Kümmerer N, Foglierini M, Serrano L. 2006 Noise in transcription negative feedback loops: simulation and experimental analysis. *Mol. Syst. Biol.* **2**, 41. (doi:10.1038/msb4100081)
23. Srinivasan S, Hu JS, Currle DS, Fung ES, Hayes WB, Lander AD, Monuki ES. 2014 A BMP-FGF morphogen toggle switch drives the ultrasensitive expression of multiple genes in the developing forebrain. *PLoS Comput. Biol.* **10**, e1003463. (doi:10.1371/journal.pcbi.1003463)
24. Wang L, Xin J, Nie Q. 2010 A critical quantity for noise attenuation in feedback systems. *PLoS Comput. Biol.* **6**, e1000764. (doi:10.1371/journal.pcbi.1000764)
25. Chen M, Wang L, Liu CC, Nie Q. 2013 Noise attenuation in the ON and OFF states of biological switches. *ACS Synth. Biol.* **2**, 587–593. (doi:10.1021/sb400044g)
26. Alarcon C *et al*. 2009 Nuclear CDKs drive Smad transcriptional activation and turnover in BMP and TGF-β pathways. *Cell* **139**, 757–769. (doi:10.1016/j.cell.2009.09.035)
27. Chung S-W, Miles FL, Sikes RA, Cooper CR, Farach-Carson MC, Ogunnaike BA. 2009 Quantitative modeling and analysis of the transforming growth factor $\beta$ signaling pathway. *Biophys. J.* **96**, 1733–1750. (doi:10.1016/j.bpj.2008.11.050)
28. Nakabayashi J, Sasaki A. 2009 A mathematical model of the stoichiometric control of Smad complex formation in TGF-β signal transduction pathway. *J. Theor. Biol.* **259**, 389–403. (doi:10.1016/j.jtbi.2009.03.036)
29. Schmierer B, Tournier AL, Bates PA, Hill CS. 2008 Mathematical modeling identifies Smad nucleocytoplasmic shuttling as a dynamic signal-interpreting system. *Proc. Natl Acad. Sci. USA* **105**, 6608–6613. (doi:10.1073/pnas.0710134105)
30. Karim MS, Buzzard GT, Umulis DM. 2012 Secreted, receptor-associated bone morphogenetic protein regulators reduce stochastic noise intrinsic to many extracellular morphogen distributions. *J. R. Soc. Interface* **9**, 1073–1083. (doi:10.1098/rsif.2011.0547)
31. Vilar JMG, Jansen R, Sander C. 2006 Signal processing in the TGF-β superfamily ligand-receptor network. *PLoS Comput. Biol.* **2**, e3. (doi:10.1371/journal.pcbi.0020003)
32. Behar M, Hoffmann A. 2013 Tunable signal processing through a kinase control cycle: the IKK signaling node. *Biophys. J.* **105**, 231–241. (doi:10.1016/j.bpj.2013.05.013)
33. Behar M, Barken D, Werner SL, Hoffmann A. 2013 The dynamics of signaling as a pharmacological target. *Cell* **155**, 448–461. (doi:10.1016/j.cell.2013.09.018)
34. Rosenfeld N, Elowitz MB, Alon U. 2002 Negative autoregulation speeds the response times of transcription networks. *J. Mol. Biol.* **323**, 785–793. (doi:10.1016/S0022-2836(02)00994-4)
35. Tyson JJ, Chen KC, Novak B. 2003 Sniffers, buzzers, toggles and blinkers: dynamics of regulatory and signaling pathways in the cell. *Curr. Opin. Cell Biol.* **15**, 221–231. (doi:10.1016/S0955-0674(03)00017-6)
36. Savageau MA. 1974 Comparison of classical and autogenous systems of regulation in inducible operons. *Nature* **252**, 546–549. (doi:10.1038/252546a0)
37. Rosenfeld N, Alon U. 2003 Response delays and the structure of transcription networks. *J. Mol. Biol.* **329**, 645–654. (doi:10.1016/S0022-2836(03)00506-0)
38. Gurdon JB, Mitchell A, Mahony D. 1995 Direct and continuous assessment by cells of their position in a morphogen gradient. *Nature* **376**, 520–521. (doi:10.1038/376520a0)
39. Dyson S, Gurdon JB. 1998 The interpretation of position in a morphogen gradient as revealed by occupancy of activin receptors. *Cell* **93**, 557–568. (doi:10.1016/S0092-8674(00)81185-X)
40. Jullien J, Gurdon J. 2005 Morphogen gradient interpretation by a regulated trafficking step during ligand-receptor transduction. *Genes Dev.* **19**, 2682–2694. (doi:10.1101/gad.341605)